The oxidation behavior of Cu42Zr42Al 8Ag8 bulk metallic glasses

Cao, W. H.; Zhang, J. L.; Shek, C. H.

Published in:
Journal of Materials Science

Published: 01/02/2013

Document Version:
Final Published version, also known as Publisher's PDF, Publisher's Final version or Version of Record

Published version (DOI):
10.1007/s10853-012-6851-y

Publication details:
Cao, W. H., Zhang, J. L., & Shek, C. H. (2013). The oxidation behavior of Cu42Zr42Al 8Ag8 bulk metallic glasses. *Journal of Materials Science*, *48*(3), 1141-1146. https://doi.org/10.1007/s10853-012-6851-y

J Mater Sci (2013) 48:1141–1146
DOI 10.1007/s10853-012-6851-y

The oxidation behavior of $Cu_{42}Zr_{42}Al_8Ag_8$ bulk metallic glasses

W. H. Cao · J. L. Zhang · C. H. Shek

Received: 10 September 2011 / Accepted: 16 January 2012 / Published online: 19 September 2012

Abstract The oxidation behavior of $Cu_{42}Zr_{42}Al_8Ag_8$ bulk metallic glass was studied in synthetic air over the temperature range of 330–460 °C. The oxidation kinetics of the metallic glass follows a single parabolic rate law at 330 and 390 °C and a two-stage parabolic rate law from 420 to 460 °C. Silver precipitates on the topmost oxide layer of the metallic glass were revealed by energy-dispersive X-ray spectroscopy together with X-ray diffraction pattern. Observation using scanning electron microscopy shows that silver metal precipitated at all temperatures and some islands were formed on the outermost copper oxide layer at high temperatures. Multilayered oxide scales were also observed with silver precipitates sandwiched between copper- and zirconium-rich oxides layers.

Introduction

Bulk metallic glasses (BMGs) have received much interest in recent years because of their importance in both theoretical studies and industrial applications. Among those BMG systems developed, Cu–Zr-based BMGs are among the most popular amorphous alloys that possess the advantages of low material cost, superior mechanical properties, and good glass-forming ability (GFA) [1–5]. Recent works reported that a Cu–Zr-based $Cu_{42}Zr_{42}Al_8Ag_8$ alloy with large critical dimensions and high fracture strengths can be prepared by copper mold casting [6, 7]. The large GFA, superior mechanical properties, and Ni-free nature, endowed such metallic glasses with potential applications in not only structural materials but also biomaterials. However, the investigations of the environmental behavior of metallic glasses in such systems are very limited [8, 9]. It was reported that elemental metals such as nickel [10], copper [11–14], and noble metal (palladium, platinum, and gold) [14–16] could be separated or precipitated out during oxidation of zirconium-containing metallic glasses. However, few investigations have been conducted on the oxidation behavior of silver containing glassy alloy. Recently, Kai et al. [9] investigated the air oxidation of $Cu_{45}Zr_{45}Al_5Ag_5$ BMGs and found the precipitation of Ag elemental metal and they suggested that the precipitation played a partly blocking effect in the oxidation of $Cu_{45}Zr_{45}Al_5Ag_5$ BMGs. In our previous investigation on oxidation behavior of $Cu_{42}Zr_{42}Al_8Ag_8$ below glass-transition temperature [17], precipitation of mushroom-like elemental silver particles was observed. However, the precipitation accelerated the oxidation instead of retarding it as suggested in $Cu_{45}Zr_{45}Al_5Ag_5$ BMGs. In this article, the oxidation kinetics of $Cu_{42}Zr_{42}Al_8Ag_8$ BMGs was investigated in detail in both glassy state and supercooled liquid state, and the precipitation behavior of Ag was also explored for better understanding.

Experimental

$Cu_{42}Zr_{42}Al_8Ag_8$ pre-alloys were prepared by arc melting the mixtures of pure Cu (99.99 wt%), Zr (99.9 wt%), Al (99.99 wt%), Ag (99.99 wt%) metals in a Ti-gettered argon atmosphere. To improve the homogeneity of the alloy, re-melting was done three times. 3 mm diameter BMG samples were produced by copper mold casting technique. The amorphous feature of the alloy was verified by X-ray diffraction (XRD). The glass-transition T_g and

W. H. Cao (✉) · J. L. Zhang · C. H. Shek
Department of Physics and Materials Science, City University of Hong Kong, Kowloon Tong, Hong Kong, China
e-mail: wenhuancao@hotmail.com

crystallization temperature T_x of the BMG are 440 and 506 °C, respectively, as measured in a purified nitrogen atmosphere with a Perkin Elmer DSC 7 using a constant heating rate of 20 K/min. The BMG samples surfaces were ground to 1200 grit, cleaned with acetone, and dried immediately before the tests. Oxidation behaviors of the BMGs over temperatures ranging from 330 to 460 °C were carried out by thermo-gravimetric analysis (TGA Q50, TA USA) in synthetic air. After oxidation, the remaining substrate alloy was examined by a Siemens D 500 diffractometer with Cu Kα irradiation ($\lambda = 0.15406$ nm). The morphology of the top surface and cross section were observed by JEOL JSM 820 scanning electron microscope (SEM). Chemical composition analysis was conducted by energy dispersive X-ray spectrometers (EDS) attached to SEM.

Results and discussion

Oxidation kinetics

Parabolic plots of the oxidation kinetics over the temperature range of 330–460 °C are shown in Fig. 1. It is clear that the oxidation reaction kinetics could be well described by a parabolic rate law, $W = kt^{1/2}$, where W is mass gain per unit area of the specimen, t the oxidation time in seconds, and k (g cm^{-2} s$^{-1/2}$) is the parabolic rate constant. The oxidation kinetics followed a single parabolic rate law at low temperature (330–390 °C), but exhibited a two-stage parabolic rate law at high temperature (420–460 °C) which consists of a fast-growth stage oxidation and then a slow-growth stage. Values of k at different temperatures and stages were fitted and listed in Table 1. The duration of the first stage was also listed in Table 1. It is clear that the duration decreased with increasing temperature. Using

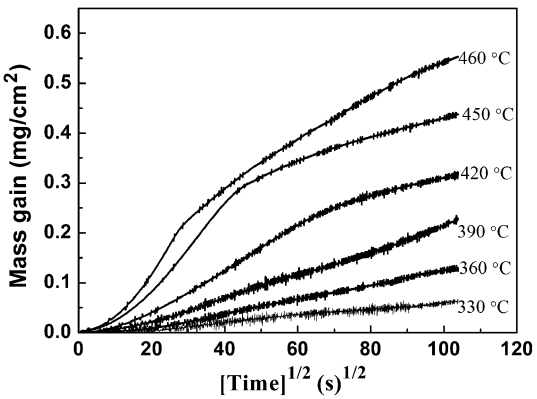

Fig. 1 Plots of mass gain (g/cm^2) versus square root of time (s$^{1/2}$) for $Cu_{42}Zr_{42}Al_8Ag_8$ BMG at various temperatures

Table 1 Variation of parabolic rate constant (k, g cm^{-2} s$^{-1/2}$) with temperature (°C) at different stages, τ(s) is the transition time between the first stage and the second stage

Temperature	k_1	k_2	τ
330	6.31×10^{-7}	–	–
360	1.46×10^{-6}	–	–
390	2.39×10^{-6}	–	–
420	4.42×10^{-6}	1.77×10^{-6}	4225
450	8.77×10^{-6}	2.09×10^{-6}	1764
460	1.05×10^{-5}	4.08×10^{-6}	806

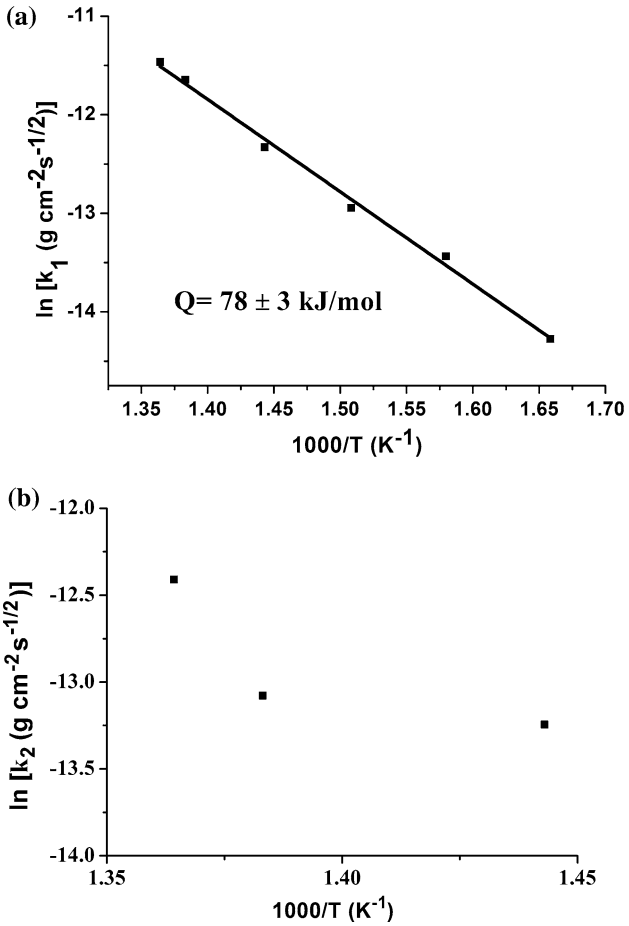

Fig. 2 Arrhenius plot between ln k (g cm^{-2} s$^{-1/2}$) and $1/T$ (10^3 K^{-1}) in the first stage **a** and in the second stage **b**. The *straight line* has been fitted among the filled points

value of k in Table 1, the activation energy Q for oxidation can be calculated with the Arrhenius equation

$$k = k_0 e^{-Q/RT},$$

where k is the parabolic rate constant, k_0 is a constant, R is the universal gas constant, and T is the oxidation temperature in Kelvin scale. Figure 2a shows the Arrhenius plot between ln (k_1) and 1000/T, where k_1 is the slope measured

from the initial linear portion of Fig. 1. All points lie on a straight line. The activation energy and pre-factor of the initial stage oxidation, related to the formation of the thin oxide layer, are calculated to be $Q = 78 \pm 3$ kJ/mol, $k_0 = 3.58$ g cm^{-2} s$^{-1/2}$, respectively. However, the points in the second stage at 420–460 °C cannot be fitted with a line as shown in Fig. 2b, which indicates that the oxidation behavior in the temperature region cannot be simply described with a single activation energy.

Microstructure and phase constitution

Figure 3 shows the corresponding XRD patterns of oxide phases formed at different temperatures. At 330 °C, it can be seen that tetragonal ZrO_2 (t-ZrO_2) and metallic Ag are dominant in the surface layer. With increased temperature, minor amounts of Al_2O_3 and copper oxides appeared. The intensities of Cu_2O and CuO peaks become stronger with further increased temperature, which indicates the enrichment of copper oxides in the oxide layer. Minor amounts of m-ZrO_2 were observed at high temperatures (420–460 °C) but absent at low temperatures (330–390 °C). The formation of m-ZrO_2 was commonly seen in the high-temperature (above T_g) oxidation of Zr-based metallic glass [18, 19]. The structures of substrates were also examined. Crystal peaks were only observed above 450 °C, as shown in Fig. 4. The dominance of ZrO_2 in the oxide layer could be explained by the activation energy for diffusion in metal oxides. The activation energy (78 ± 3 kJ/mol) for oxidation of $Cu_{42}Zr_{42}Al_8Ag_8$ metallic glass obtained in this study is roughly close to the value for diffusion of oxygen in ZrO_2 (86.9 kJ/mol) [20], suggesting that the oxidation of $Cu_{42}Zr_{42}Al_8Ag_8$ metallic glass in the first stage might be controlled by the oxygen diffusion in ZrO_2. Similar results were also obtained in $Cu_{60}Zr_{30}Ti_{10}$ BMGs but at lower temperatures [21]. To investigate the oxidation behavior in

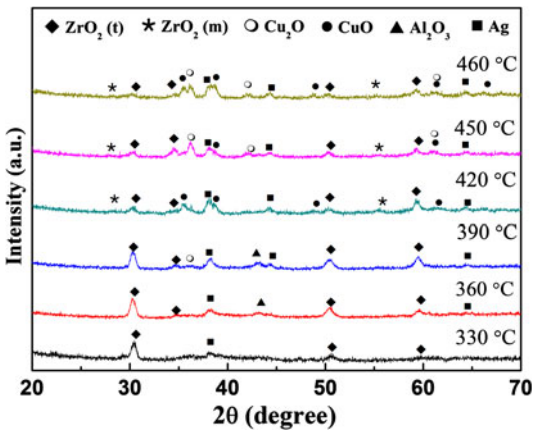

Fig. 3 XRD patterns of oxide scales obtained at 330, 360, 390, 420, 450, and 460 °C

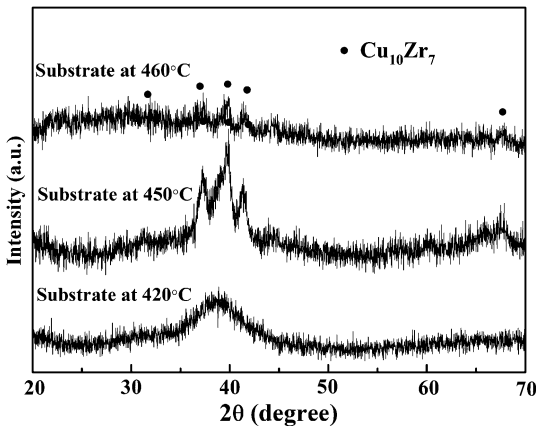

Fig. 4 XRD spectra of the substrate in the $Cu_{42}Zr_{42}Al_8Ag_8$ BMG oxidized at 420, 450, and 460 °C

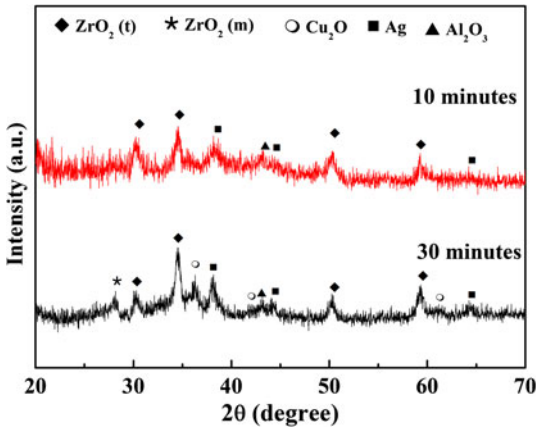

Fig. 5 XRD spectra of the scales formed on the $Cu_{42}Zr_{42}Al_8Ag_8$ BMG oxidized at 450 °C for various durations

the second stage at high temperatures, different short-term oxidation tests were performed at 450 °C. XRD analyses of the oxide scales produced by the exposure of the amorphous sample are shown in Fig. 5. It is obvious that, in the first 10 min, t-ZrO_2 and Ag were the main products formed on the surface, although minor Al_2O_3 was also detected. After the first stage oxidation ($\tau = 1764$ s) for 30 min, little m-ZrO_2 and Cu_2O phases were detected. With further oxidation, the amount of Cu_2O phases increased and CuO phase appeared (Fig. 3). From the above results, it is concluded that the growth of CuO/Cu_2O is responsible for the second-stage oxidation behavior at $T \geq 420$ °C.

Figure 6 shows the surface morphologies of specimens after oxidation at different temperatures. As seen in Fig. 6a, some white precipitates were formed along the grinding grooves on the oxidized sample surface at 330 °C. The particles might be Ag as predicted from the XRD spectra in Fig. 3. After further oxidation at 390 °C, many large hemispherical white precipitates were observed (Fig. 6b). EDS analysis showed that the white precipitates

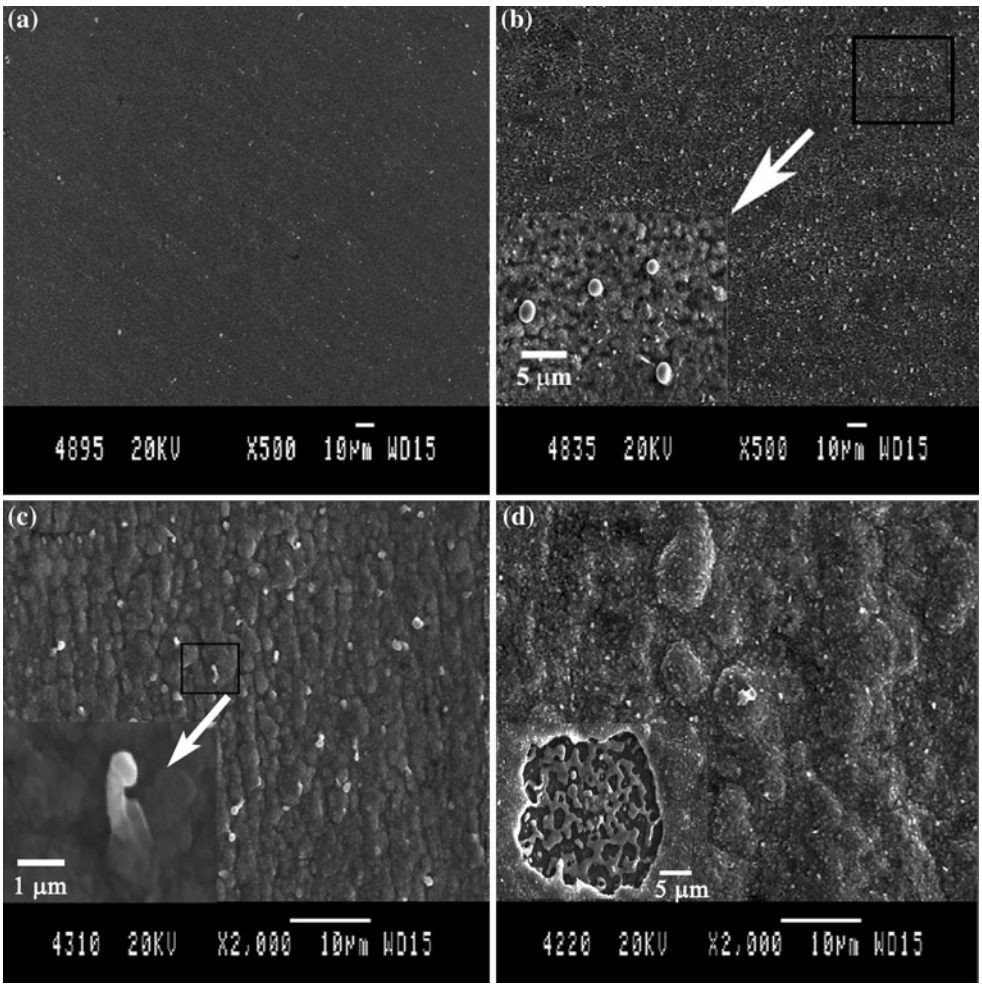

Fig. 6 Surface morphologies of $Cu_{42}Zr_{42}Al_8Ag_8$ metallic glass oxidized at **a** 330 °C, **b** 390 °C, **c** 420 °C, **d** 450 °C

were almost pure silver (~92 %). The products around the silver precipitates are mainly composed of copper, corresponding to copper oxides. At 420 °C, mushroom-like precipitates which are similar to that formed on the ribbon counterpart were occasionally seen on the surface, as shown in Fig. 6c. Small Ag–metal channels through the oxide scale might exist, as observed in [17]. These channels could enhance the inward diffusion of oxygen. The high oxidation tendency of amorphous alloys with noble-metal-containing was also found in references [14–16]. It was explained that in the noble-metal-containing amorphous alloy, the high oxidation rate is due to the large atomic size of noble metals which leads to an increase of the vacant space, facilitating higher oxygen diffusivity [14]. Meanwhile, the accelerated oxidation can also found in crystalline alloys with certain noble metals concentrations in which internal oxidation occurs [22, 23]. Although noble metals have low affinity for oxygen, the interface between the alloy and the internal oxide particles (internal oxidation zone) enhanced oxygen diffusion.

After oxidization at 450 °C, little white mushroom-shaped particles were observed and many copper oxide islands were found on the surface (Fig. 6d). As seen from the inset in Fig. 6d, an area with the island-like topmost layer (copper oxides) peeled off and this shows that many precipitates were embedded beneath. According to the EDS results, the precipitates are mainly composed of silver. Besides, many openings around the silver precipitates were observed, which is consistent with the discrete distribution of the hemispherical silver shown in Fig. 6b. From the above results, it could be inferred that the oxidation process starts with the formation of ZrO_2 followed by the precipitation of silver particles. As explained by Zhang et al. [17] that silver mostly existed as solute in Zr, once Zr was oxidized to ZrO_2, pure metal silver will precipitate out due to the high enthalpy of formation for the silver oxide in the temperature range used in this study [24]. The weak boundaries or vacancies induced by oxidation are promising segregation sites for the expelled Ag. Meanwhile, the copper remaining in the matrix tended to move outward to

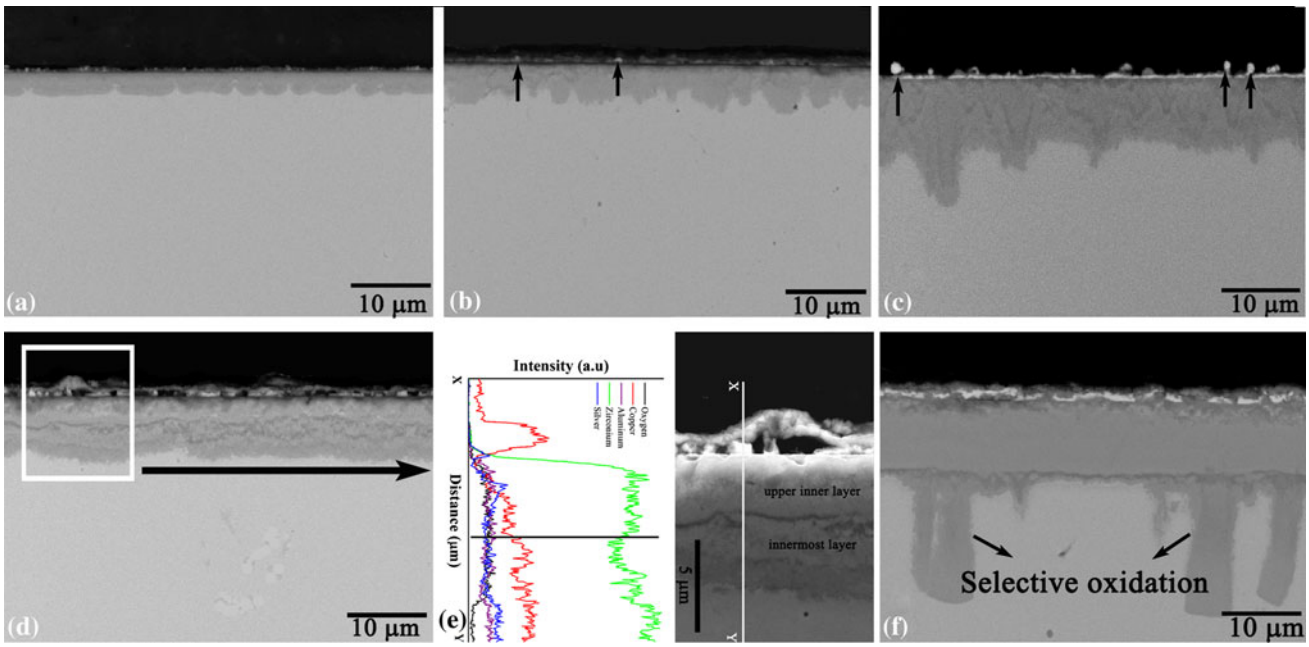

Fig. 7 Cross section BE image of samples oxidized at **a** 360 °C, **b** 390 °C, **c** 420 °C, **d** 450 °C, **e** magnified area in (**d**) and corresponding EDS line profile, **f** 460 °C

form oxides along the grinding grooves. The internal stress induced by volume expansion squeezed the hemispherical silver precipitates to produce a mushroom-like morphology. With increasing temperature, copper ions move faster than silver due to its smaller atomic size, and finally, the copper oxides covered the silver precipitates underneath.

Figure 7 shows SEM micrographs in back-scattered-electron-image (BEI) mode of the cross sections of specimens oxidized from 360 to 460 °C. There are two oxide layers at 360 °C (Fig. 7a), 390 °C (Fig. 7b), and 420 °C (Fig. 7c) and the thickness of the scale increased with increasing temperature. The outer layer mainly contains Ag (with arrows below) and Cu, which is in agreement with the observation of the top surface. A rugged oxide–alloy interface between the matrix and the inner layer was clearly seen from 360 to 420 °C. It is probably due to the combined effect of outwards diffusion of the copper and the silver in the alloy [25]. The outward diffusion of Cu and Ag from the alloy to the oxide leads to open space in the glassy lattice. In order to fill the space, the alloy may deform plastically and move inward. Similar observations were also found in Zr–Cu–Al–Ni [26] and Cu–Zr–Al [27] metallic glasses.

After oxidation at 450 °C, a sandwich multilayer was observed, as shown in Fig. 7d. According to the results of EDS line profile (Fig. 7e), the island-like outermost layer is Cu-rich, the middle layer with white precipitates is silver-rich, and the inner layer is mainly Zr-rich. The inner layer can be further divided into two layers. The upper inner layer has lower copper content than that in the innermost layer. As the topmost layer is mainly composed of copper, we speculate that the lower content of copper in the upper inner layer is due to the fast outward diffusion of copper to the topmost layer. It is also the reason that silver precipitates were seldom observed on the top surface at high temperatures. The increased copper oxides at the topmost layer indicate that the rate-controlling step in the second-stage oxidation process at higher temperatures is the outward diffusion of copper. Meanwhile, the upper inner layer has a higher content of silver than that in the innermost layer as indicated by the appearance of a peak in the EDS line profile. This suggests that many silver particles may be embedded in the zirconium oxide. Similar observations were also found in Zr–Pd and Zr–Au metallic glasses [14–16]. The average thickness of the oxide scale at temperature 450 and 460 °C is 7.6 ± 1 and 9.8 ± 1 μm, respectively. Selective oxidation with formation of oxide protrusions on the substrate was observed at 460 °C (Fig. 6f). It can be attributed to the coarse crystallized substrate as the oxidation is preferred in certain orientations of the grain or along grain boundaries [28].

As far as the difference in oxidation behavior between the glassy state and the supercooled liquid state was concerned, although the oxidation kinetics in both states follows the parabolic law and is controlled by the diffusion of O and Cu, the oxidation rates are quite different. Oxidation rate is much higher in the supercooled liquid state (in the initial period, see Fig. 1). This is due to not only the temperature effect but also a faster diffusion in the supercooled liquid state [29, 30]. The gradual slows down of

oxidation rate at high temperatures can be attributed to two reasons. One is the thick oxide scale, which increased the diffusion distance between the oxygen ions and the metal ions. The other one is possibly related to the crystallization of metallic glasses [31]. This point was testified by many comparative studies that the mass gain of amorphous alloys is considerably larger than that of the crystallized alloy in the temperature region corresponding to the supercooled liquid state [21, 26].

Conclusions

The oxidation behavior of $Cu_{42}Zr_{42}Al_8Ag_8$ BMGs over the temperature range of 330–460 °C was studied. Several conclusions can be drawn as follows:

1. Oxidation kinetics of the $Cu_{42}Zr_{42}Al_8Ag_8$ BMG alloy follow a single parabolic law at 330–390 °C, but a two-stage parabolic rate law at 420–460 °C.
2. The oxidation products at low temperature primarily consist of t-ZrO_2 and Ag, while Cu_2O and CuO are dominant oxides at high temperatures. The oxidation behavior at low temperature and the first stage at higher temperatures is controlled by the inward oxygen diffusion, while outward diffusion of copper is responsible for the second-stage oxidation behavior at $T \geq 420$ °C.
3. The surface morphology of the sample shows that discrete silver particles were precipitated out. The Ag particle changed from hemispherical to mushroom-like shape, and finally was embedded below by copper oxides formed at high temperatures.
4. Two-layer scales were observed at $T \leq 420$ °C and the sandwiched silver precipitates were formed between the copper- and the zirconium-rich oxides at $T \geq 450$ °C.

Acknowledgements This study was supported by a Strategic Research Grant (Project number 7008101) from City University of Hong Kong.

References

1. Kim YJ, Busch R, Johnson WL, Rulison AJ, Rhim WK, Isheim D (1994) Appl Phys Lett 65:2136
2. Lin XH, Johnson WL (1995) J Appl Phys 78:6514
3. Inoue A, Fan C (1999) Nanostruct Mater 12:741
4. Inoue A (2000) Acta Mater 48:279
5. Fan GJ, Freels M, Choo H, Liaw PK, Li JJZ, Rhim WK, Johnson WL, Yu P, Wang WH (2006) Appl Phys Lett 89:241917
6. Zhang QS, Zhang W, Inoue A (2006) Scripta Mater 55:711
7. Sung DS, Kwon OJ, Fleury E, Kim KB, Lee JC, Kim DH, Kim YC (2004) Met Mater Int 10:575
8. Zhang W, Zhang QS, Qin CL, Inoue A (2008) Mater Sci Eng, B 148:92
9. Kai W, Ren IF, Kao PC, Wang RF, Chuang CP, Freels MW, Liaw PK (2009) Adv Eng Mater 11:380
10. Maciejewskit M, Baiker A (1990) J Chem Soc, Faraday Trans 86:843
11. Tam CY, Shek CH (2006) J Mater Res 21:851
12. Kilo M, Hund M, Sauer G, Baiker A, Wokaun A (1996) J Alloy Compd 236:137
13. Kudelski A, Janik-Czachor M, Bukowska J, Pisarek M, Szummer A (2002) Mater Sci Eng, A 326:364
14. Kimura HM, Asami K, Inoue A, Masumoto T (1993) Corros Sci 35:909
15. Jastrow L, Köster U, Meuris M (2004) Mater Sci Eng, A 375–377:440
16. Inoue A, Masumoto T, Itabahi S (1986) Sci Rep Ritu A 33:183
17. Zhang JL, Cao WH, Shek CH (2011) J Alloys Compd 509:S219
18. Hsieh HH, Kai W, Huang RT, Pan MX, Nieh TG (2004) Intermetallics 12:1089
19. Kai W, Ho TH, Hsieh HH (2008) Metall Mater Trans A 39:1838
20. Schneider S, Sun X, Nicolet M-A, Johnson WL (1995) Diffusion. West Point Military Academy, New York
21. Tam CY, Shek CH (2005) J Mater Res 20:1396
22. Danielewski M, Grzesik Z, Mrowec S (2001) Corros Sci 53:2785
23. Douglass DL (1995) Oxid Met 44:81
24. Gaskell DR (2003) Introduction to the thermodynamics of materials, 4th edn. Taylor & Francis, New York
25. Wagner C (1956) J Electrochem Soc 103:371
26. Kai W, Hsieh HH, Nieh TG, Kawamura Y (2002) Intermetallics 10:1265
27. Tam CY, Shek CH, Wang WH (2008) Rev Adv Mater Sci 18:107
28. Birks N, Meier GH (1983) Introduction of high temperature oxidation of metals, 2nd edn. Edward Arnold, London
29. Knorr K, Macht MP, Freitag K, Mehrer HJ (1999) J Non-Cryst Solids 669:250
30. Zumkley T, Naundorf V, Macht MP, Frohberg G (2002) Ann Chim Sci Mater 27:55
31. Liu L, Chan KC (2005) Appl Phys A 80:1737